COMMUNICATION

Hydrogenated $Li_4Ti_5O_{12}$ Nanowire Arrays for High Rate Lithium Ion Batteries

Laifa Shen, Evan Uchaker, Xiaogang Zhang, and Guozhong Cao**

Due to their unique characteristics in terms of high energy densities, lithium ion batteries (LIBs) employed for small electronic devices are now being extended to large applications such as cordless power tools and electric vehicles (EV).[1,2] However, current LIBs using graphite as the anodic material exhibit poor rate performance induced by their low Li diffusion coefficient, poor cycle life and serious safety issues caused by the solid electrolyte interphase (SEI) film.[3,4] Developing high-performance electrodes materials has been an essential component of the current endeavor for the next generation of LIBs.

In the search for safe materials with good rate capability and excellent cyclic stability, spinel $Li_4Ti_5O_{12}$ (LTO) has been extensively studied as an ideal anodic material for LIBs owing to several inherent advantages.[5–10] LTO exhibits an extremely flat discharge and charge plateaus at about 1.55 V vs Li/Li^+, which makes it safe by avoiding the SEI formation.[11–13] Also, as a zero-strain insertion material, LTO can accommodate up to three lithium ions per molecule with no volume change.[14,15] These features render it a promising candidate for anodic electrodes for LIBs. However, the main disadvantage that restricts the application of LTO is the low electronic conductivity, resulting in poor rate capability of the cells.[16–19] The most common problem-solving strategy employed in the literature is to tailor the particle size of electroactive materials to the nanometer-scale[20,21] and to enhance electronic conductivity with a surface conductive coating.[22–24] Carbon-based coating via chemical vapor deposition or a hydro/solvothermal process is the most widely used. For example, Shen et al.[24] reported the fabrication of LTO/C microspheres through a simple one-step solvothermal route. Because of safety issues concerning carbon materials, more attention has been directed to carbon-free methods to improve electronic conductivity. Park et al.[25] synthesized nitridation-driven conductive LTO using ammonia gas to decompose the LTO surface. Very recently, Wang et al.[26] reported the utility of rutile-TiO_2 as a carbon-free nanocoating to improve the kinetics of LTO toward fast lithium insertion/extraction.[26] LTO nanostructures, such as nanoparticles and nanosheets, have been extensively studied in the hope of achieving a short transportation distance for both lithium ions and electrons. However, LTO nanostructures need to be mixed with a binder and carbon black and further pressed onto electrode substrates before they are assembled into batteries. Not only does this process increase additional undesirable interfaces in the electrode but also inevitably compromises the overall energy storage capacity. Recently, self-supported nanowire arrays (NWAs) growing directly on a current-collecting substrate, such as Co_3O_4 nanowire arrays growing on Ti foil,[27] have been reported to overcome the drawbacks of mixing with conductive carbon and have fast charging/discharging.[28] However, free-standing and well-aligned LTO 1D nanostructures with improved electronic conductivity growing directly on current-collecting substrate have not been realized. Such materials would greatly simplify the fabrication and processing of electrodes by directly and intimately connecting to the charge collecting substrates with much improved rate capability. Therefore, it is highly desirable to design and fabricate novel LTO 1D nanostructure arrays with improved electronic conductivity directly on current-collecting substrates.

In this work, for the first time, we describe a facile template-free route to fabricate $Li_4Ti_5O_{12}$ nanowire arrays (LTO NWAs) growing directly on Ti foil and enhance its electronic conductivity by creating Ti^{3+} sites through hydrogenation. When used as anodes for LIBs without any ancillary materials, the as-synthesized hydrogenated $Li_4Ti_5O_{12}$ nanowire arrays (H-LTO NWAs) manifest an excellent rate capability and a significantly enhanced cycling performance.

The schematics shown in **Figure 1** illustrate the formation steps of the H-LTO NWAs. Firstly, $H_2Ti_2O_5 \cdot H_2O$ NWAs with an average diameter of ≈80 nm grow directly on Ti foil through an alkali hydrothermal process combined with an ion-exchange process (see the Supporting Information, Figure S1 and S2). Then, the L-T-O (LTO precursor) NWAs were in situ formed by chemical lithiation of $H_2Ti_2O_5 \cdot H_2O$ NWAs in LiOH solution. An annealing treatment in Ar/H_2 at different temperatures is utilized to convert the precursor into spinel LTO and create Ti^{3+} sites to enhance its electronic conductivity. In this new concept of self-supported H-LTO NWAs electrodes, the well-aligned LTO NWAs electrodes possess large specific space that facilitates the fast transfer of Li^+. The electronic conductivity of LTO NWAs are significantly improved by controlled introduction of Ti^{3+} states via hydrogenation and there is direct connection to the growth substrate, which ensures every nanowire participates in the ultrafast electrochemical reaction. Additionally, the use of binders or any conducting additive material is avoided in this

L. F. Shen, Prof. X. G. Zhang
College of Material Science and Engineering
Nanjing University of Aeronautics and Astronautics
Nanjing 210016, China
E-mail: azhangxg@nuaa.edu.cn
L. F. Shen, E. Uchaker, Prof. G. Z. Cao
Department of Materials Science and Engineering
University of Washington
Seattle, WA 98195, USA
E-mail: gzcao@u.washington.edu

DOI: 10.1002/adma.201203151

unique electrode architecture. All of these factors contribute to the effective ambipolar diffusion of Li^+ and e^- into/out of LTO in the H-LTO NWA electrode architecture, enabling remarkable rate capability and cycling performance.

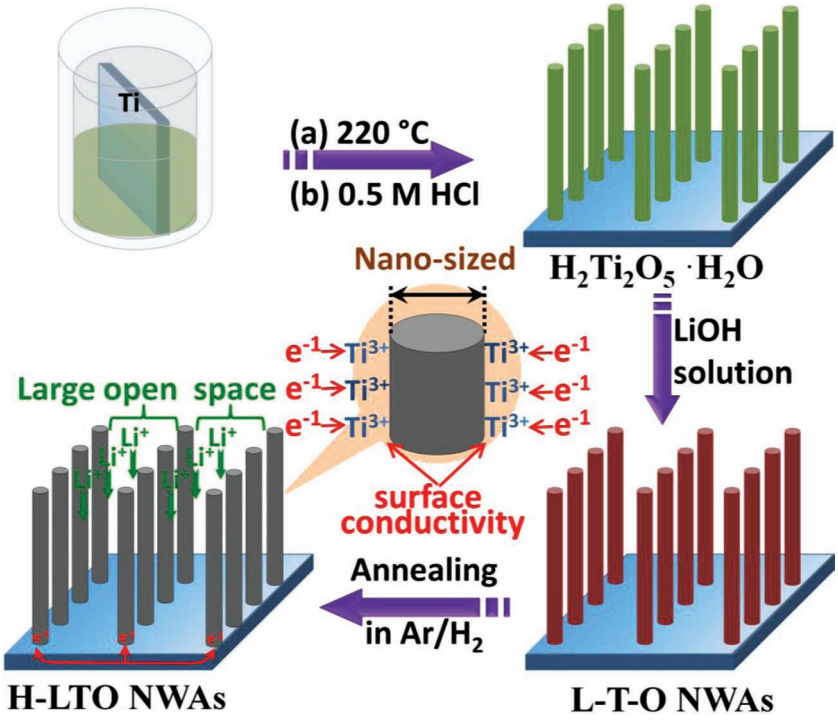

Figure 1. Schematic illustration for the fabrication of H-LTO NWAs.

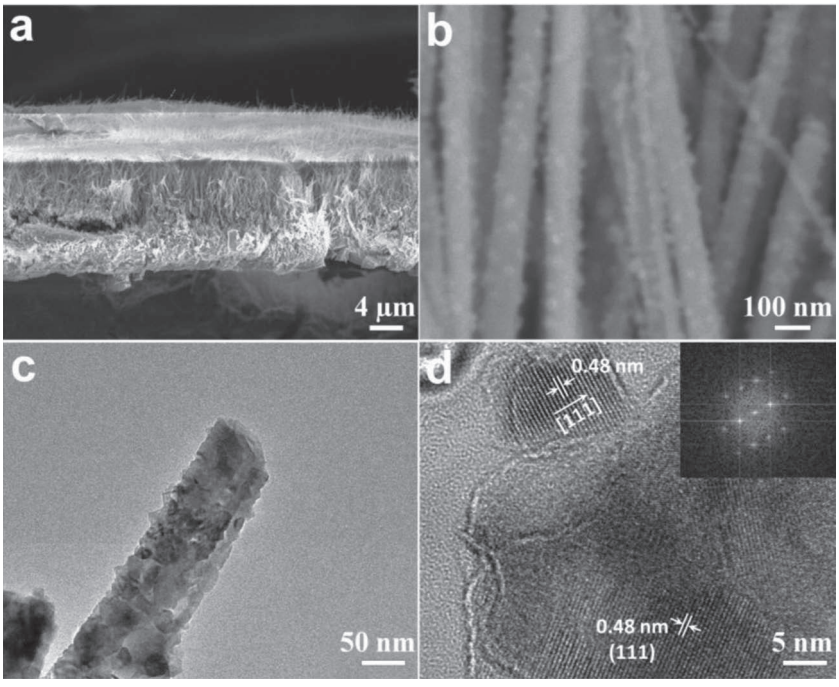

Figure 2. a,b) Cross-sectional SEM images of H-LTO NWAs annealing at 600 °C. c,d) TEM images of H-LTO NWAs annealing at 600 °C.

The morphology of the nanowire arrays was examined with scanning electron microscopy (SEM) and transmission electron microscopy (TEM). As shown in **Figure 2**a,b, the H-LTO film has a highly oriented 1D structure with a typical column diameter of 90 nm and length of about 8 μm. Unlike smooth $H_2Ti_2O_5 \cdot H_2O$ nanowires, some ultrathin nanoparticles attached on the surface of H-LTO nanowires, which may increase the effective surface area, providing more active sites for electrochemical reactions. In addition, the large open space between neighboring nanowires allows facile electrolyte diffusion throughout the thin film electrode. The SEM images of LTO NWAs are shown in Figure S3 (Supporting Information), which have the same morphology as H-LTO NWAs. Figure 2c reveals that a typical H-LTO nanowire is actually a hierarchically porous nanowire composed of many small nanoparticles instead of the conventional single-crystal nanowire, which was also confirmed by HRTEM image (Figure 2d). A lattice spacing of 0.48 nm was observed, in a good agreement with the d-spacing of 0.484 nm associated with the (111) direction of spinel structure (ICDD 00-049-0207). The fast Fourier transform (FFT) pattern taken along the (111) zone axis (inset of Figure 2d) also confirmed the formation of a highly crystallized spinel phase.

X-ray diffraction (XRD) was used to identify the crystallographic structure; the results are shown in **Figure 3**a. With the exception of the reflections owing to metallic titanium, all Bragg peaks of the both samples are consistent with those of the LTO phase (JCPDS Card No. 49-0207). No residues or parasitic phases were detected, indicating that the $H_2Ti_2O_5 \cdot H_2O$ NWAs completely convert to spinel LTO after chemical lithiation and post-annealing. Detailed peak broadening analysis of the (111) XRD reflection using the Scherrer equation indicates that the average crystallite size is approximately 18 nm; this result further suggests that the nanowires are composed of nanocrystalline subunits and corroborated by the TEM results. XRD studies (Figure S4, Supporting Information) reveal that the LTO precursor could be transformed to the spinel LTO phase after heat treatment at 500 °C, significantly lower than the solid-state reaction. The peak intensity increases but there is no phase change for H-LTO NWAs when the hydrogenation temperature increases from 500 to 700 °C.

The effect of hydrogenation on the chemical composition of LTO NWAs was analyzed using X-ray photoelectron spectroscopy (XPS). XPS survey spectra collected from pristine and hydrogenated LTO NWAs

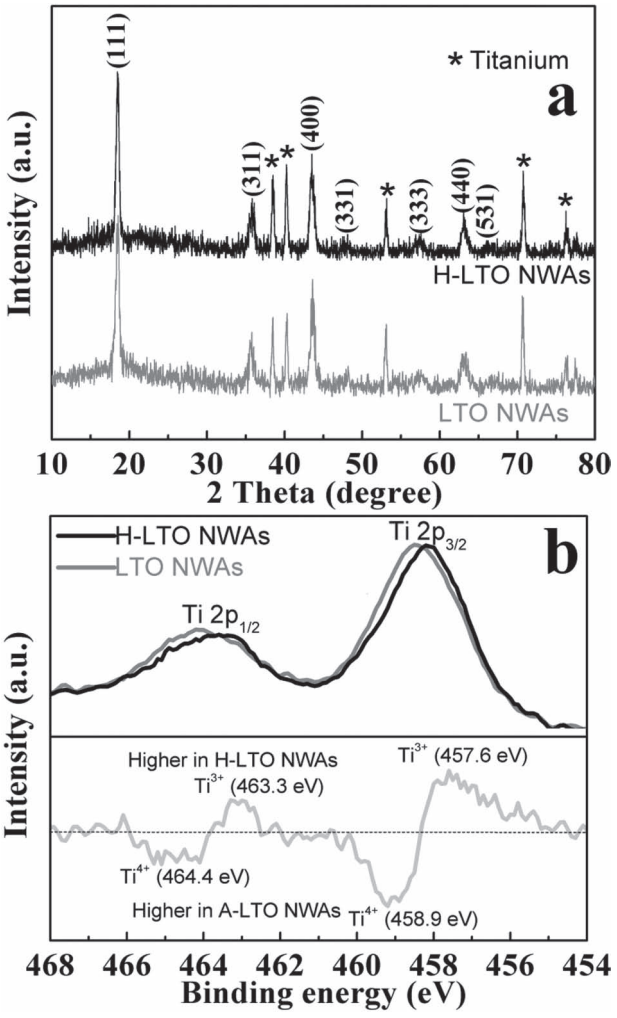

Figure 3. a) XRD pattern of H-LTO NWAs and LTO NWAs annealing at 600 °C. b) Overlay of normalized Ti 2p core level XPS spectra of H-LTO NWAs and LTO NWAs, together with the difference in their spectra ("H-LTO NWAs" minus " LTO NWAs").

treated at 600 °C are very similar (Figure S5a, Supporting Information). The high-resolution Ti 2p XPS core level XPS spectra of pristine and hydrogenated LTO NWAs are shown in Figure 3b. Two broad peaks centered at ≈464.4 and ≈458.9 eV correspond well with characteristic Ti $2p_{1/2}$ and Ti $2p_{3/2}$ peaks of Ti^{4+} in both samples.[29,30] Compared with the XPS spectrum of Ti 2p of pristine LTO NWAs, a small negative shift can be observed in the XPS spectrum of hydrogenated LTO NWAs, demonstrating that treatment with hydrogen caused a change of surface bonding of LTO nanowires. By subtracting the normalized Ti 2p spectra of H–LTO NWAs with pristine LTO NWAs, two extra peaks appeared at ≈463.3 and ≈457.6 eV are attributed to Ti $2p_{1/2}$ and Ti $2p_{3/2}$ peaks of Ti^{3+},[31,32] suggesting the Ti^{3+} sites were successful created in H–LTO NWAs during hydrogenation. The O 1s core level XPS spectra of LTO NWAs and H-LTO NWAs were also recorded and compared in Figure S5b (Supporting Information). Unlike the single O 1s peak at ≈530.3 eV for LTO NWAs, the H-LTO NWAs exhibit a broader O 1s peak that can be resolved into two peaks at ≈530.3 and ≈531.9 eV. An additional peak appeared at ≈531.9 eV was attributed to the presence of Ti–OH bonds, which has been reported to be located at ≈1.5–1.8 eV higher binding energy corresponding to the Ti–O.[33]

Coin-type cell configuration was used to evaluate the electrochemical properties of H-LTO NWAs as an anode, and the results were compared with a pristine LTO NWAs sample. **Figure 4**a shows the discharge profiles of H-LTO NWAs cycled at different current rates from 0.2 to 30 C in the voltage range of 1.0–2.5 V. At a low C-rate (e.g., 0.2 C), the electrode achieved a first discharge capacity as high as ≈173 mA h g^{-1}, which is very close to the theoretical capacity of 175 mAh g^{-1}. In addition, the electrode showed a flat voltage plateau at the potential of ≈1.55 V ascribable to the redox of Ti^{4+}/Ti^{3+} couple. As the current rate increased from 1 to 5 and 10 C, the discharge capacity slightly decreased from 166 to 157 and 145 mA h g^{-1}, respectively. At the high rate of 30 C (5.3 A g^{-1}), the capacity retained ≈69% of the value achieved at 0.2 C with a discharge voltage plateau at 1.33 V, indicating the excellent rate capability of the material. However, the pristine LTO had no clear discharge voltage plateau and the capacity was only 83 mA h g^{-1} at the rate of 20 C (Figure 4b). The rate performance of pristine LTO and H-LTO NWAs at various charge–discharge rates were compared in Figure 4c. At 0.2 C rate, the pristine LTO NWAs exhibits high initial discharge capacity (164 mA h g^{-1}), followed however by a sharp capacity decay with the increase of current rate. H-LTO NWAs, however, exhibited much higher lithium-ion storage capacity and much better rate capability than pristine LTO NWAs. For instance, at a rate of 30 C, the capacity of H-LTO NWAs was more than 3 times greater than LTO NWAs. Moreover, the H-LTO NWAs electrode possesses better cyclic stability than pristine LTO NWAs (Figure 4d). After 100 cycles the discharge capacity of the H-LTO NWAs was 149 mA h g^{-1} at 5 C with only ≈5% capacity loss, while for pristine LTO NWAs, the corresponding values were 107 mA h g^{-1} and ≈9%. Although the capacities decrease with increasing C-rate, the H-LTO NWAs still show a high capacity with excellent capacity retention even at the high rate of 10 C (Figure S6, Supporting Information). Hydrogenation effectively enhanced lithium-ion storage capacity and improved storage kinetics, particularly at high C rates.

A comparison of the cyclic voltammogram (CV) curves for pristine LTO NWAs and H-LTO NWAs is shown in Figure 4e. It should be noted that the peak shape of H-LTO NWAs was sharper and intense, and the gap between redox peaks was smaller than that of pristine LTO NWAs, demonstrating that the former had lower overall resistance and greater efficiency of the redox reaction. This low ionic and electronic resistance collaborated well with the electrochemical impedance spectroscopy results presented in Figure 4f. In Table S1 (Supporting Information) of the ESI, the H-LTO NWAs electrode shows a much lower charge-transfer resistance than that of the pristine LTO NWAs electrode (43.8 vs 121.7 Ω) on the basis of the modified Randles equivalent circuit given in the inset of Figure 4f. Furthermore, the exchange current densities ($i^0 = RT/nFR_{ct}$) of the H-LTO NWAs cell were higher than those of the LTO

NWAs. The fast charge-transfer kinetics of H-LTO NWAs electrode could be attributed to Ti^{3+} groups which enhanced the conductivity of the electrode.

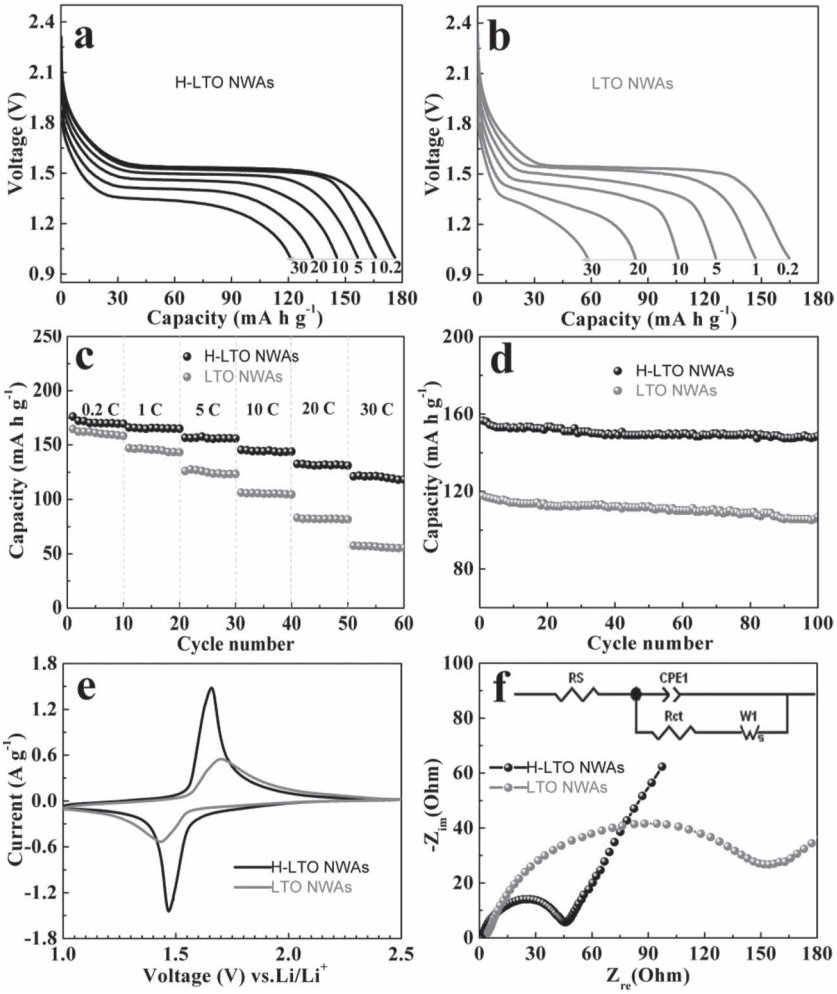

Figure 4. Comparison of Electrochemical properties of LTO and H-LTO NWAs: the discharge curves of a) H-LTO NWAs and b) LTO NWAs. c) Specific discharge capacities at various C rates. d) Cycling performances at the rate of 5 C. e) Cyclic voltammograms. f) Nyquist plots.

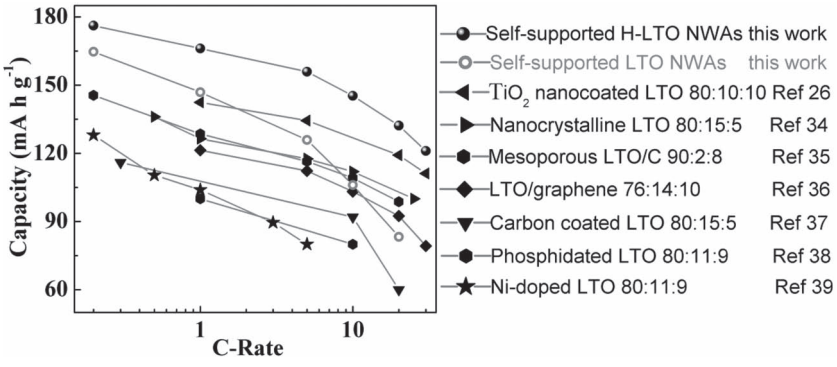

Figure 5. Comparison of rate capability of H-LTO NWAs with other LTO based high-rate electrodes reported recently. The capacities were estimated based on their total mass of electrode material. Their electrode compositions are listed using the mass ratio of active materials: conductive carbon: binder.

We also compared this work with other LTO based high-rate electrodes reported in the recent literature, including rutile-TiO_2 nanocoated,[26] nanocrystalline,[34] the formation of nanocomposites with mesoporous carbon[35] and graphene,[36] carbon coated,[37] surface phosphidated,[38] doped LTO,[39] and the results are shown in **Figure 5**. A large fraction of polymer binders and conductive agents that do not contribute to lithium storage capacity were used in fabrication of traditional LTO-based high rate electrode, resulting in low electrode storage density. For example, nanocrystalline LTO electrode manifest a capacity of 158 and 147 mA h g^{-1} at 1 and 5 C, respectively. If corrected by considering the total electrode mass (excluding the current collector), its actual capacity deceases to 126 and 118 mA h g^{-1}, respectively. By comparison, well-aligned LTO NWAs growing directly on Ti foil without any additive exhibited comparable electrochemical performance to commonly conductive coating electrodes, which was attributed mainly to the large space that facilitate the fast transfer of Li^+ and small diameter of NW that provides the short diffusion length. Due to the unique nanostructure and greatly enhanced electrical conductivity enabling the fast migration of both lithium ions and electrons to reach the interior of each NW, the H-LTO NWAs electrode yields much batter rate capability than LTO NWAs and other LTO based high rate electrode. As a result we can emphasize that if electrodes are appropriately designed and fabricated, for example with nanostructures and surface defects, there would be no need to add conductive additive and binders to achieve high energy/power density.

In summary, we have rationally designed and fabricated self-supported LTO NWAs architectures by a facile solution chemical approach. Importantly, a conceptually straightforward approach is developed to further enhance lithium storage capacity by introducing Ti^{3+} in LTO nanowires through hydrogenation. The high electrical conductivity of H-LTO NWAs as compared with pristine LTO NWAs results in their high capacity (173 mA h g^{-1} at 0.2 C), excellent rate capability (121 mA h g^{-1} at 30 C), and good cyclic stability (≈5% capacity loss after 100 cycles at a rate of 5 C). Creating surface defects is a very simple yet very effective approach to enhancing ion or/and electron conductivity, it may also be extended to other anode and cathode materials. These important findings could open up new opportunities for LTO in constructing high-performance binder free energy storage devices.

Experimental Section

Materials Synthesis: In a typical procedure, a piece of titanium foil (1 cm × 2 cm) ultrasonically cleaned in water, acetone and ethanol for 15 min, respectively, was placed against the wall of a 50 mL Teflon-lined stainless steel autoclave was filled with 20 mL 1 M NaOH aqueous solution and then kept at 220 °C for 16 h. After hydrothermal growth, the titanium foil covered with nanowire array was taken out and immersed in 0.5 M HCl solution for 1 h to replace Na^+ with H^+. Then, the $H_2Ti_2O_5{\cdot}H_2O$ nanowire arrays grown on Ti foil was immersed in 2 M LiOH solution and kept at 60 °C for 8 h. After rinsing with copious amounts of deionized water and drying under ambient conditions, the titanium foil covered with L-T-O nanowires was calcined in Ar or 5% v/v H_2 in Ar at various temperatures ranging of 500–700 °C for 1.5 h.

Materials Characterization: The crystal structure of the obtained samples was characterized by X-ray diffraction (XRD) (Bruker D8 advance) with Cu Kα radiation. The microstructural properties were characterized using transmission electron microscopy (TEM) (TEM, FEI, Tecnai-20, USA), high-resolution transmission electron microscopy (HRTEM, JEOL JEM-2010), and scanning electron microscopy (SEM, JEOL, JSM-7000). The X-ray photoelectron spectroscopy (XPS) analysis was performed on a Perkin-Elmer PHI 550 spectrometer with Al Kα (1486.6 eV) as the X-ray source.

Electrochemical Measurement: Electrochemical characterization was performed in coin type cells, which were assembled in an argon-filled glove box using the LTO NWAs assembly as the work electrode and Li metal as the counter and reference electrode. The two electrodes were electronically separated with polypropylene (PP) film as the separator. A 1 M $LiPF_6$ solution in a 1:1 (v/v) mixture of ethylene carbonate (EC) and dimethyl carbonate (DMC) was used as the electrolyte. Finally, the cells were aged for 12 h before the measurements. The cells were galvanostatically charged and discharged using an Arbin battery tester BT-2000 (Arbin Instruments, College Station, Texas). Cyclic voltammetry (CV) studies were carried out on an electrochemical workstation (CH Instruments, model 605B). The AC impedance spectrum was measured using a Solatron 1260 impedance analyzer in the frequency range ≈10^{-2}–10^6 Hz.

Supporting Information

Supporting Information is available from the Wiley Online Library or from the author.

Acknowledgements

This work was supported by the National Science Foundation (USA) (CMMI-1030048), the National Natural Science Foundation of China (No. 21173120) and the Natural Science Foundation of Jiangsu Province (BK2011030). L.S. also thanks the Outstanding Doctoral Dissertation in NUAA (BCXJ11-10) for financial support and the China Scholarship Council (CSC) for providing a scholarship for Ph.D. study at the University of Washington.

Received: August 1, 2012
Revised: September 3, 2012
Published online: October 5, 2012

[1] J. M. Tarascon, M. Armand, *Nature* **2001**, *414*, 359.
[2] J. Tollefson, T. Scully, A. Witze, O. Morton, *Nature* **2008**, *454*, 818.
[3] Y. K. Sun, S. T. Myung, B. C. Park, J. Prakash, I. Belharouak, K. Amine, *Nat. Mater.* **2009**, *8*, 320.
[4] S. B. Yang, X. L. Feng, K. Müllen, *Adv. Mater.* **2011**, *23*, 3575.
[5] E. Ferg, R. J. Gummow, A. Dekock, M. M. Thackeray, *J. Electrochem. Soc.* **1994**, *141*, L147.
[6] X. Lu, L. Zhao, X. He, R. Xiao, L. Gu, Y. S. Hu, H. Li, Z. Wang, X. Duan, L. Q. Chen, J. Maier, Y. Ikuhara, *Adv. Mater.* **2012**, *24*, 3233.
[7] W. J. H. Borghols, M. Wagemaker, U. Lafont, E. M. Kelder, F. M. Mulder, *J. Am. Chem. Soc.* **2009**, *131*, 17786.
[8] L. F. Shen, C. Z. Yuan, H. J. Luo, X. G. Zhang, K. Xu, F. Zhang, *J. Mater. Chem.* **2011**, *21*, 761.
[9] E. Kang, Y. S. Jung, G. H. Kim, J. Y. Chun, U. Wiesner, A. C. Dillon, J. K. Kim, J. Lee, *Adv. Funct. Mater.* **2011**, *21*, 4349.
[10] J. Kim, J. Cho, *Electrochem. Solid-State Lett.* **2007**, *10*, A81.
[11] G. G. Amatucci, F. Badway, A. D. Pasquier, T. Zheng, *J. Electrochem. Soc.* **2001**, *148*, A930.
[12] T. Ohzuku, A. Ueda, N. Yamamoto, *J. Electrochem. Soc.* **1995**, *142*, 1431.
[13] L. F. Shen, X. G. Zhang, H. S. Li, C. Z. Yuan, G. Z. Cao, *J. Phys. Chem. Lett.* **2011**, *2*, 3096.
[14] L. Aldon, P. Kubiak, M. Womes, J. Jumas, J. Olivier-Fourcade, J. Tirado, J. Corredor, C. P. Vicente, *Chem. Mater.* **2004**, *16*, 5721.
[15] J. Haetge, P. Hartmann, K. Brezesinski, J. Janek, T. Brezesinski, *Chem. Mater.* **2011**, *23*, 4384.
[16] L. F. Shen, C. Z. Yuan, H. J. Luo, X. G. Zhang, K. Xu, Y. Y. Xia, *J. Mater. Chem.* **2010**, *20*, 6998.
[17] G. N. Zhu, H. J. Liu, J. H. Zhuang, C. X. Wang, Y. G. Wang, Y. Y. Xia, *Energy Environ. Sci.* **2011**, *4*, 4016.
[18] L. F. Shen, E. Uchaker, C. Z. Yuan, P. Nie, M. Zhang, X. G. Zhang, G. Z. Cao, *ACS Appl. Mater. Interfaces* **2012**, *4*, 2985.
[19] G. Du, N. Sharma, V. K. Peterson, J. A. Kimpton, D. Jia, Z. Guo, *Adv. Funct. Mater.* **2011**, *21*, 3990.
[20] J. M. Feckl, K. Fominykh, M. Doblinger, D. Fattakhova-Rohlfing, T. Bein, *Angew. Chem. Int. Ed.* **2012**, *51*, 7459.
[21] J. Lim, E. Choi, V. Mathew, D. Kim, D. Ahn, J. Gim, S. H. Kang, J. Kim, *J. Electrochem. Soc.* **2011**, *158*, A275.
[22] L. Zhao, Y. S. Hu, H. Li, Z. Wang, L. Q. Chen, *Adv. Mater.* **2011**, *23*, 1385.
[23] H. G. Jung, S. T. Myung, C. S. Yoon, S. B. Son, K. H. Oh, K. Amine, B. Scrosati, Y. K. Sun, *Energy Environ. Sci.* **2011**, *4*, 1345.
[24] L. F. Shen, C. Z. Yuan, H. J. Luo, X. G. Zhang, L. Chen, H. S. Li, *J. Mater. Chem.* **2011**, *21*, 14414.
[25] K. S. Park, A. Benayad, D. J. Kang, S. G. Doo, *J. Am. Chem. Soc.* **2008**, *130*, 14930.
[26] Y. Wang, L. Gu, Y. G. Guo, H. Li, X. Q. He, S. Tsukimoto, Y. Ikuhara, L. J. Wan, *J. Am. Chem. Soc.* **2012**, *134*, 7874.
[27] Y. G. Li, B. Tan, Y. Y. Wu, *Nano Lett.* **2008**, *8*, 265.
[28] X. Xue, S. Yuan, L. Xing, Z. Chen, B. He, Y. Chen, *Chem. Commun.* **2011**, *47*, 4718.
[29] X. Chen, L. Liu, P. Y. Yu, S. S. Mao, *Science* **2011**, *331*, 746.
[30] G. M. Wang, H. Wang, Y. Ling, Y. Tang, X. Yang, R. C. Fitzmorris, C. Wang, J. Z. Zhang, Y. Li, *Nano Lett.* **2011**, *11*, 3026.
[31] Y. Liu, J. M. Szeifert, J. M. Feckl, B. Mandlmeier, J. Rathousky, O. Hayden, D. Fattakhova-Rohlfing, T. Bein, *ACS Nano* **2010**, *4*, 5373.
[32] X. H. Lu, G. M. Wang, T. Zhai, M. H. Yu, J. Gan, Y. X. Tong, Y. Li, *Nano Lett.* **2012**, *12*, 1690.
[33] E. McCafferty, J. P. Wightman, *Surf. Interface Anal.* **1998**, *26*, 549.
[34] A. S. Prakash, P. Manikandan, K. Ramesha, M. Sathiya, J. M. Tarascon, A. K. Shukla, *Chem. Mater.* **2010**, *22*, 2857.
[35] L. F. Shen, X. G. Zhang, E. Uchaker, C. Z. Yuan, G. Z. Cao, *Adv. Energy Mater.* **2012**, *2*, 691.
[36] L. F. Shen, C. Z. Yuan, H. J. Luo, X. G. Zhang, S. D. Yang, X. J. Lu, *Nanoscale* **2011**, *3*, 572.
[37] Y. G. Wang, H. M. Liu, K. Wang, H. Eiji, Y. Wang, H. S. Zhou, *J. Mater. Chem.* **2009**, *19*, 6789.
[38] M. R. Jo, K. M. Nam, Y. Lee, K. Song, J. T. Park, Y. M. Kang, *Chem. Commun.* **2011**, *47*, 11474.
[39] J. Kim, S. W. Kim, H. Gwon, W. S. Yoon, K. Kang, *Electrochim. Acta* **2009**, *54*, 5914.